IEEE Access
Multidisciplinary | Rapid Review | Open Access Journal

Received April 17, 2019, accepted May 27, 2019, date of publication June 5, 2019, date of current version June 24, 2019.

Digital Object Identifier 10.1109/ACCESS.2019.2921089

On the Electromagnetic Wave Behavior Due to Partial Discharge in Gas Insulated Switchgears: State-of-Art Review

AHMAD DARWISH[1], SHADY S. REFAAT[2], HAMID A. TOLIYAT[1], AND HAITHAM ABU-RUB[2]
[1]Electrical Engineering Department, Texas A&M University, College Station, TX 77843, USA
[2]Electrical Engineering Department, Texas A&M University, Doha, Qatar

Corresponding author: Ahmad Darwish (a.darwish1993@tamu.edu)

This work was supported by the Qatar National Research Fund (a member of the Qatar Foundation) under Grant [10-0101-170085].

ABSTRACT The rapid growth of gas insulated switchgears as a compact, efficient, and reliable device has recently been given great attention. Albeit gas insulated switchgears can seldom suffer from failure due to the high resiliency and robustness, some severe damages have been experienced by such devices particularly in the event of partial discharge. Thus, monitoring such accidents has become a vital part of power systems reliability. The ultra-high frequency techniques have recently shown superior performance in the detection and classification of electromagnetic waves produced by partial discharge. This is mainly due to the great immunity to the noise of the ultra-high frequency detection techniques compared with the very-high-frequency counterparts. This review paper highlights the mathematical aspects of the electromagnetic waves generated by partial discharge. It also delivers an overview of the electromagnetic wave behavior in the complex structure of gas insulated switchgears, and outlines the important characteristics of the internal and external partial discharge detection using ultra-high frequency methods.

INDEX TERMS Electromagnetic waves behavior, finite difference time domain, gas insulated switchgears, partial discharge, sensors, ultra-high frequency measurements.

I. INTRODUCTION

The determination of whether power utilities suffer from high levels of Partial Discharge (PD) is an important factor that contributes to the safety of neighboring utilities, economic and customer satisfaction, and the avoidance of regulatory fines. Thus, a careful management of such capital assets has become an important objective for different power firms [1]. PD occurs when the electric field stress inside an insulator exceeds its breakdown strength due to the high applied voltage, an ionization of atoms could possibly take place producing a high-frequency transient current inside the insulation material [2], [3]. Even though PDs might be initially very small, the generated current might gradually cause chemical decomposition of the insulator causing erosion with time. Eventually, the moving charges might bridge between the two electrodes connecting the insulator. This can cause a full breakdown or failure of the device. There are different PD sources that take place inside an insulator including but not limited to overvoltage, lightning strikes, aging, and internal manufacturing defects [4].

Different medium voltage (MV) and high voltage (HV) power equipment have different types of PD defects. These defects can be classified based on the location of occurrence as corona discharge, surface discharge, and internal discharge. Corona discharge takes place in the presence of sharp edges or coarse surfaces of electrodes in MV or HV equipment. The existence of corona discharge contributes to the enhancement of electric field at these tips due to the accumulation of charges. It initiates a dramatic stress increase on the insulation material. Surface Discharge on the other hand arises when current flows through a conductor due to a high voltage difference between two electrodes. When the current flows along one of the electrodes, charges might accumulate at the sharp edges causing a breakdown on the surface of the insulator. An important factor that contributes to the event of surface discharge is that the insulation material has to have higher permittivity than the surrounding material [5]. Internal discharge usually takes place inside oil-filled MV and HV power devices. Such discharge usually occurs

The associate editor coordinating the review of this manuscript and approving it for publication was Qammer Hussain Abbasi.

due to the existence of a small cavity inside the insulation material with weaker dielectric strength and lower permittivity than its surrounding. Consequently, the stress caused by the electric field is stronger around the cavity causing ionization and breakdown of the dielectric material. Another common discharge type is caused by floating metals inside Gas Insulated Switchgear (GIS) systems. The behavior of this type of defect is similar to that of corona discharge since the working principle is similar. When small metallic particles are located inside a GIS, charges will accumulate at sharp tips causing enhancement of the electric field which might, as a consequence, cause PD [5], [6].

GIS devices are made up of an inner high voltage conductor, an insulator (usually Sulfur Hexafluoride (SF6)), an outer tank, and other high voltage components including switches, transformers and circuit breakers. SF6 has been widely used in many gas insulated electrical equipment due to its high insulation properties and breakdown voltage stress. The later property is coming from the fact that SF6 is an electronegative material which can easily capture low energy electrons [7]. Moreover, such gaseous material could be used to detect the different types of PDs based on the characteristic of the generated decomposed materials. A review paper on the detection of PD type based on the decomposition of SF6 has been published in [8].

GISs are widely used in power system utilities because of the high reliability, safety, robustness, environmental aspects, and reduced space [9], [10]. Such devices have been commercially introduced in the 1970s and are widely used in substations. Many GISs are getting aged nowadays and the need to mitigate failure has recently become of paramount importance for researchers. Maintenance facilities have shifted from time based monitoring to condition based monitoring, where different diagnostic techniques for the detection of different defects such as PDs are used [11], [12]. Around 85% of the failures of HV and MV equipment are mainly attributed to PDs [15]. This highlights the significance of giving PD analysis more attention to improve power systems reliability. The most commonly types of defects found in GIS includes protrusions, floating metals, particle on a spacer surface, and void on a solid spacer [13]–[15].

Various off-line and on-line non-conventional techniques have been developed in the last few decades for the detection and localization of PD. Such techniques include chemical, acoustic, optical, and electrical methods. These techniques are developed based on formation of ozone, emission of acoustic waves, production of light due to ionization, and the emission of electromagnetic (EM) waves respectively [16]–[19]. Each of the aforementioned techniques has its own benefits and drawbacks. Chemical techniques, which can be either off-line or on-line, rely on the collection of products or gases emitted due to the PD defect. Two different methodologies are widely used for chemical detection namely high performance liquid chromatography (HPLC) and dissolved gas analysis (DGA). Chemical methods suffer from lack of localization of defects despite its high sensitivity. Moreover, it does not work properly unless sufficient amount of expelled products or gases are collected increasing the required detection time [16]. Acoustic techniques are mainly on-line techniques. They locate PDs based on the acoustic signal amplitude and phase delay. This method relies on the detection of mechanical waves produced by the rapid energy release due to the vaporization of the insulating materials. The main disadvantage of this method is that it might give a false location for PD defects due to interferences from the environment [17], [18]. Optical techniques, which are also mainly on-line techniques, show superior performance when it comes to PD detection and localization since they have great immunity to different electromagnetic interferences coming from the environment. Optical techniques rely on the intrinsic interferometers. Nevertheless, such devices suffer from random polarization causing fringe fading issues [17], [19].

Electrical techniques are widely used and depend on non-invasive methods. Non-conventional electrical methods can be classified into two main categories namely the usage of high frequency current transformer (HFCT) and Ultra-High Frequency (UHF) sensors. Both techniques are usually classified as on-line techniques. HFCTs are devices capable of detecting the current pulses using inductive coils along with ferromagnetic cores. Such devices are widely used for the detection of PD in cables by connecting the HFCT around the grounding cable. They are used to detect signals with frequency spectrum of around 3MHz to 30MHz. The main drawback of the use of HFCT is the fast attenuation of high frequency signals due to the low pass filtering behavior of cables [20]. UHF techniques, which are based on the detection of signals covering frequencies from 0.3GHz to 3GHz, are widely used in the detection of PDs in GISs. In such devices, when a PD occurs, an EM wave will be radiating due to the acceleration and deceleration of electrons. Such EM waves contain the Transverse Electro-Magnetic (TEM) mode as well as other higher order modes of propagation [20].

A third electrical technique was also proposed by Collinson and Jennings to overcome some of the drawbacks associated with the UHF, HFCT and the conventional PD measuring techniques [21]. The basic idea of the technique, called Transient Earth Voltage (TEV), is that an induced pulse-like EM wave is to be generated at the metallic tank of GIS in the event of PD. Thus, the usage of non-intrusive sensor mounted of the outer surface of the GIS is possible. Nevertheless, such technique suffers from the high external noise collected with the produced EM waves at different frequencies due to occurrence PD [21].

Understanding the behavior of the emitted EM waves in GIS is hard since the GIS provides a complicated structure to the propagating signals. This is mainly due to the multiple resonances created inside the GIS in addition to the different discontinuity types [22]. Although electrical techniques have a relatively good immunity to noise, they have a limited ability to locate the exact position of PD [23].

The main contribution of this paper is to provide an overview on the characteristics of the detected UHF electromagnetic waves generated by partial discharge inside GIS devices. It also discusses the behavior that EM waves exhibits inside GIS due to the complex structure of such equipment. Therefore, the paper is organized as follows: In section 2, a brief description of the PD process, some mathematical representations of PD pulses, and the frequency response of such pulses are presented. Section 3 delivers some mathematical models related to the generation of EM waves by PD. A detailed description of the EM wave behavior due to the different elements of GIS is given and discussed in section 4. Next, the different connection methodologies of sensors used in the detection of UHF signals is carried out in section 5. To sum up, the paper aims to deliver a detailed analysis on the EM wave behavior detected using the UHF sensors in GISs due to PDs.

II. PARTIAL DISCHARGE MECHANISMS AND MODELS IN GIS

A. PARTIAL DISCHARGE MECHANISMS

In GIS, the phenomenon of partial discharge is mainly governed by two mechanisms namely Townsend and Streamer. Depending on the size of the discharge, either Townsend or both mechanisms govern the PD phenomenon. For any of the aforementioned mechanisms to take place inside a GIS, an ionized electron has to exist between two electrodes with potential difference. Electron ionization could be defined as the process of releasing an electron from a molecule producing a positive ion and a negative ion. There are many factors that could cause the ionization process to take place including but not limited to light exposition, thermal effects, or solar radiations [24].

1) TOWNSEND MECHANISM

When free electrons reside between an anode and a cathode, an electric field is applied at the free electrons forcing them to accelerate towards the anode due to the applied. Due to this force, the electrons start to gain kinetic energy while moving between the two electrodes. If electrons collide with some other atoms with enough kinetic energy, new ionized electrons are released leaving positive ions behind. Due to this process, the number of electrons reaching the anode is larger than the number of liberated electrons at the cathode and hence electric current starts to increase [24]. If the temperature is fixed, the accumulation of energy by an electron is proportional to the applied electric field and the free mean path (FMP). FMP is defined as the effective distance an atom can travel between 2 consecutive collisions, and is inversely proportional to pressure [25].

Under the applied electric field, electrons will be moving towards the anode. They leave positive charges behind forming an avalanche. The positive ions will be accelerating towards the opposite side (the cathode), but at slower velocities than electrons since they are heavier in weight.

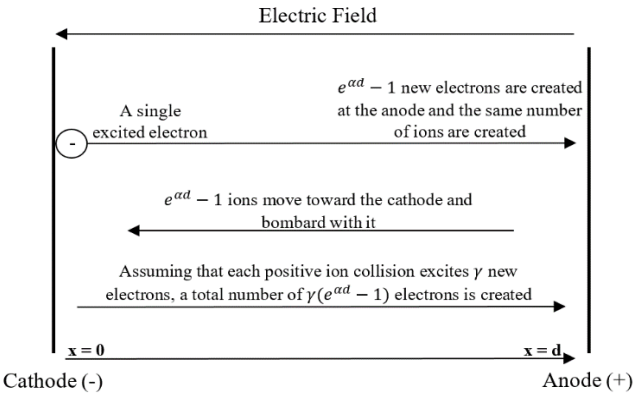

FIGURE 1. Townsend mechanism process.

When the positive ions reach the cathode and collide with it, new moving electrons will be generated. The total number of electrons excited due to Townsend mechanism is:

$$N_e(x) = N_{ec} e^{\alpha x} \tag{1}$$

where N_e is the total number of electrons located at distance x from the cathode, N_{ec} is the number of liberated electrons in addition to the generated electrons due to the bombardment of positive ions with the cathode, and α is the Townsend first ionization coefficient. α could be defined as the number of ionizing collisions that can take place during the movement of an electron [25], [26]. It is a strong function of the applied electric field and its value is usually obtained experimentally. Fig. 1 shows the Townsend mechanism due to the excitation of an initial electron located at the cathode (x = 0) which travelled a distance d to reach the anode. The total number of electrons that reaches the anode is $e^{\alpha d} - 1$ new electrons (excluding the original excited electron) based on (1).

2) STREAMER MECHANISM

When gaps between electrodes get larger, Townsend mechanism can no longer explain the behavior of the avalanche, and the breakdown is not attributed only to the ionization process, but there is also the space charge and the formulation of photons. When avalanche breakdown takes place in large gaps or voids, positive and negative charges distort the field forcing electrons to move towards the tip of the avalanche and positive ions towards the tail [27]. In addition, the created photons enhance the discharge phenomenon by imposing new electrons to produce new avalanches ahead of the original one. The Streamer mechanism can be divided into three sub categories based on the gap length namely Streamer inception, Streamer propagation, and Leader propagation. If sufficient number of electrons are excited due to ionization, space charge, and photoionization, Streamer inception takes place. The field in this case is weakly non-uniform. On the other hand, Streamer propagation takes place when the gap gets larger. The most important characteristic of this type is that the field is strongly inhomogeneous. Finally, Leader propagation usually takes place when the gap gets

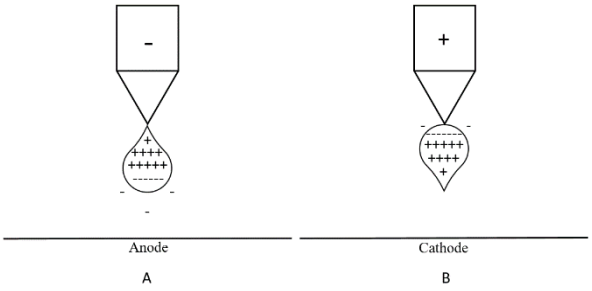

FIGURE 2. Arc modeling for Non-Uniform Gaps (Protrusion defect Model). a) Negatively charged Protrusion b) Positively Charged Protrusion.

very large [25]–[28]. No further details on the categories of Streamer mechanism is given on this paper, but readers can refer to [25]–[28] for more details.

As mentioned earlier, a protrusion defect is one of the most commonly types of defects found in GIS devices. In [10], a Finite Difference Time Domain (FDTD) model for the protrusion defect has been proposed as a relatively long needle with a very sharp tip to improve the electric field intensity. Consequently, the avalanches are formed at the tip as shown in Fig. 2. When the voltage applied at the needle is positive, electrons in the avalanche are concentrated at the non-uniform electrode whereas the positive ions are on the other side. This distribution makes the effective gap length looks smaller since the positive ion concentration looks like an extension to the non-uniform electrode, and thus, lower voltage is required for the flashover [26]. Similar concept could also be applied to the floating metal since charge concentration will be higher at the small tips of floating metals. For the case of floating metal, the PD will have a sharper pulse and broader frequency spectrum based on an experiment carried out in [29].

B. PARTIAL DISCHARGE MODELS

PD measurements have been widely used to assess the condition of the different power equipment and components including power transformers, cables, and switchgears. During the event of PD, electrons experience acceleration and deceleration. This behavior results in electromagnetic waves radiation as will be discussed in section III. Inside the complicated structure of GIS, EM waves experience high degrees of reflections and attenuation [22]. Consequently, the EM waves travel along the GIS in multiple paths making it difficult to predict the behavior of such signals.

Different types of defects generate different PD pulses. Nevertheless, most of these generated pulses have a short time-domain representation. Such pulses have a relatively large bandwidth because of the inverse relationship between the time-domain and the frequency-domain representation of a signal as shown in Fig. 3 [1], [5], [30]. Although the Gaussian pulse with larger width has initially higher spectral energy compared with its counterpart, the spectral intensity started to attenuate at lower frequency as depicted in Fig. 3b.

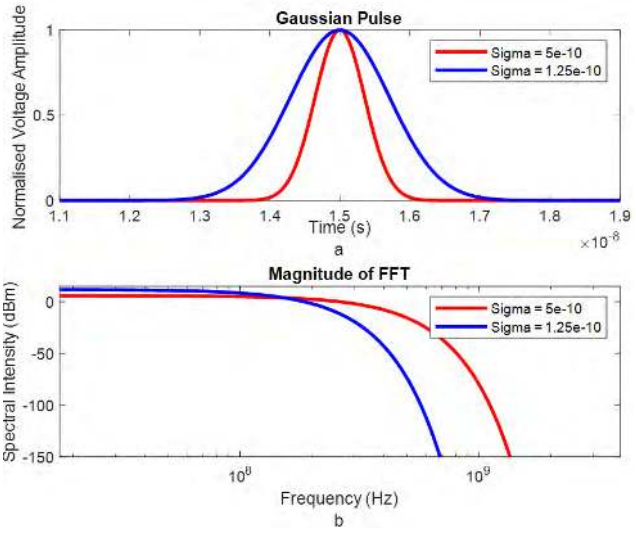

FIGURE 3. a) Time Domain and b) Frequency Domain representation of a Gaussian Pulse.

The PD pulses could mainly be modelled using one of the following equations [31]:

- Gaussian Pulse (G_0 *or* G_1) is given by:

$$G_0 = I_0 e^{\frac{-t^2}{2\sigma^2}} \tag{2}$$

where I_0 is the pulse amplitude, σ is a parameter that determines the pulse width. Equation (2) can also be represented as [10]:

$$G_1 = I_0 e^{-\frac{(t-b)^2}{c^2}} \tag{3}$$

where b is the center of the pulse, and c is used to determine the width of the pulse.

- Wanninger Pulse (W) is given by:

$$W = \frac{I_0}{T} e^{\frac{1-t}{T}} \tag{4}$$

where T is used for the determination of the pulse width.

- Double Exponential Pulse (DE) is given by:

$$DE = I_0 \left[(1+\alpha t)\, e^{-\alpha t} - (1+\beta t)\, e^{-\beta t} \right] \tag{5}$$

where α *and* β are constants used to determine the shape of the pulse.

PD due to a defect in a GIS cannot be modelled as a simple hardwiring since the wavelength of the UHF EM waves can be comparable to the size of the equipment. Thus, modeling the PD defect as a dipole antenna can provide better approximation since the gap size is usually much smaller than the size of the equipment [32].

III. ELECTROMAGNETIC WAVE RADIATION DUE TO PARTIAL DISCHARGE

The phenomenon of partial discharge is responsible for the emission of electromagnetic waves as it imposes electrical forces on electrons. The main goal of this section is to elucidate the radiation action of EM waves due to partial discharge.

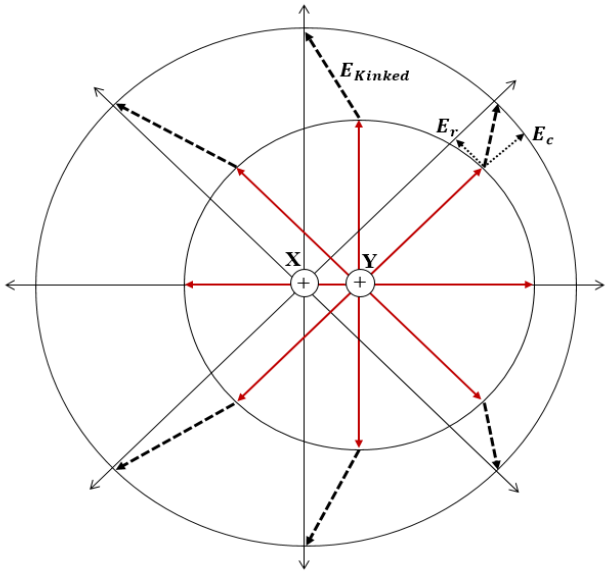

FIGURE 4. EM Wave Radiation Due to an Accelerated Charge.

A. ELECTROMAGNETIC WAVE RADIATION DUE TO POINT CHARGE AND THE LARMOR'S FORMULA

Static charges can either act as sources or sinks for electric field. Nevertheless, they do not emit EM waves because no magnetic field is created when there is no flowing current [33]. Moreover, charged particles moving at a constant velocity do not radiate EM waves in the radial direction away from the charge [5]. An essential condition for the radiation of the electromagnetic waves is the decaying behavior of the EM energy which has to be a function of the squared of the distance from the source to satisfy the poynting vector [34].

On the other hand, the acceleration and deceleration of charged particles emit EM waves. Consider a positively charged particle that starts accelerating in SF6 from rest at point X until it reaches point Y. Then, the particle stays at constant velocity as shown in Fig. 4. When the charged particle is at point X, or at an arbitrary point after point Y, no EM waves will be emitted as mentioned earlier. On the other hand, while the particle is accelerating, the electric field lines will experience 'kinking' effect to maintain the continuity condition of the electric field (since the electric field is due to the same charge). The formed 'kinks' create disturbance in the emitted field causing radiation. The radiation is a consequence of the E_r component of the kinked electric field shown in Fig. 4. It should be noted that there is no E_r field component along the direction of motion which explains why no EM waves are radiating along the direction of motion. With the assumption that the charged particle is moving at a constant velocity after point Y, the radiated electric and magnetic fields are given by [35]:

$$E_t = \frac{Q\mu_0}{4\pi}\frac{asin(\theta)}{\rho} = \frac{Qasin(\theta)}{4\pi c^2\rho\epsilon_o} \tag{6}$$

$$H_t = \frac{Q}{4\pi c}\frac{asin(\theta)}{\rho} \tag{7}$$

where Q is the charge of the particle, a is the retarded acceleration, c is the speed of light, θ is the angle between the acceleration direction and the observation point, μ_0 is the permeability of air, and ρ is the distance travelled by the electric field after some time (t). It should be noted that μ_0 is used since the permeability of air and SF6 are identical from the practical point of view. The radiated electric field behavior of an accelerated charge is similar to that of a dipole based on (6) and (7). That is, the radiation pattern of accelerated or decelerated particles could be modelled as donut shaped or toroidal radiation pattern [34]. The poynting vector could be directly computed using E and H as:

$$S = E_t \times H_t = \epsilon_0 c E_t^2 = \frac{Q^2a^2}{16\pi^2\epsilon_0\rho^2c^3}sin\,(\theta) \tag{8}$$

where ϵ_0 is the permittivity of air. Finally, the loss in the total energy can be found by integrating S over all directions. This would give the Larmor's Formula which is given by:

$$P = \frac{Q^2a^2}{6\pi c^3\epsilon_0} \tag{9}$$

where P is the total radiated power due to an accelerated/decelerated charged particle [36].

B. ELECTRIC DIPOLE MODEL OF SHORT GAPS

When an insulating void defect exists inside the spacer of a GIS, the electric dipole moment is created. The creation of dipoles is attributed to the fact that charges of opposite directions are separated by a small distance. Indeed, the apparent charge detected using the conventional methods is not the real charge (Q) but rather it is related to $Q.d$, where d is the gap length.

The electric dipole can radiate electromagnetic waves based on the Hertz vector, and the electric field is given by [37], [38]:

$$E_x = \frac{\mu_0 p}{2\sqrt{2e}\pi^{1.5}t_0^2D}f\left(\frac{t-\frac{y}{c}}{t_0}\right) \tag{10}$$

where $f\left(\frac{t-\frac{y}{c}}{t_0}\right) = \sqrt{2e}\left(\frac{t-\frac{y}{c}}{t_0}\right)e^{-\left(\frac{t-\frac{y}{c}}{t_0}\right)^2}$, $p = Q.d$ is the electric dipole moment, t_0 is a constant that depends on the Gaussian pulse width, D is the distance between the dipole and the origin, and e is the electron charge. Equation (10) shows that the radiation field intensity is inversely proportional to the pulse width. Moreover, the radiated EM wave is a function of time and a single coordinate component.

IV. ELECTROMAGNETIC WAVE BEHAVIOR INSIDE GIS TANKS

Insulation spacers and screws were used in the past to connect the compartments of GIS. Thus, the outer tanks of GIS do not provide perfect grounding for the EM waves since tanks are not perfect coaxial waveguides. In the event of PD, such configuration would result in leakage of EM waves outside the tank [9]. The apertures act as slot antennas allowing

the electric field to propagate outside the tank at resonance frequencies. Recently, the use of basin-type insulators with an external metallic cover is prevalent. Such spacer type provides better grounding for the GIS tank, prevents spacer corrosion with air, and reduces EM waves from leaking outside the tank in the event of PD [9], [39].

A GIS is a complex structure that has many different types of structural components which can largely affect the EM waves propagating inside the tank. Those discontinuities include but not limited to ground switches and disconnectors, spacers, L-shaped and T-shaped sections, and sudden changes in the inner and/or outer conductor diameter(s). In the event of PD, the relative angle between the PD source and the antenna placement also affect the EM wave behavior. Understanding the impact of the aforementioned discontinuities on EM waves has thus become of paramount importance; especially if the UHF techniques are used in the detection of PD events [22].

A. RELATIVE ANGLE BETWEEN PD SOURCE AND ANTENNA POSITION

A detailed mathematical derivation for the EM wave behavior due to PD has been carried out in [40]. The intensity of the electric field inside a simple GIS with no discontinuities depends on the dimensions of the coaxial waveguide, magnitude of the PD, and the angular position between the source and the sensor. The angular position affects the higher order modes but has no impact on the Transverse Electromagnetic (TEM) propagation mode. The TEM mode due to PD is maximum at the inner conductor and decays as we move towards the outer conductor. On the other hand, the field intensity of the higher order modes approaches a minimum when the angle between the source and the probe approaches 90° whereas it is maximum when the angle is 0° [40]–[42]. Moreover, the time-domain representation of the detected signal is not a Gaussian pulse as the case of the PD source. This is due to the fact that the field undertakes an infinite number of paths to reach the sensor, and a small portion of the wave moves directly from the source to the sensor [40].

The impact of probes placement inside GIS tanks through the use of Finite Difference Time Domain (FDTD) method have been extensively studied [43]. Probe couplers are sensors modelled to obtain the voltage amplitude inside the GIS enclosure. This is achieved by modeling each probe as a matched load with certain length to a 50-ohm coaxial line. The probe was initially inserted at 4 different locations along the radial axis ($\theta = 0$) shown in Fig. 5. The best allocation for the probe is near the outer tank to ensure that there is enough voltage difference between one end of the probe and the other. Moreover, if Transverse Magnetic (TM) mode of propagation is of interest, the probe has to be placed parallel to the longitudinal axis (z-axis) of the GIS since the electric field will have a component along that direction.

B. L-SHAPED STRUCTURE

Reflections due to the radiation of EM waves during the event of PD can largely affect the signal behavior. One

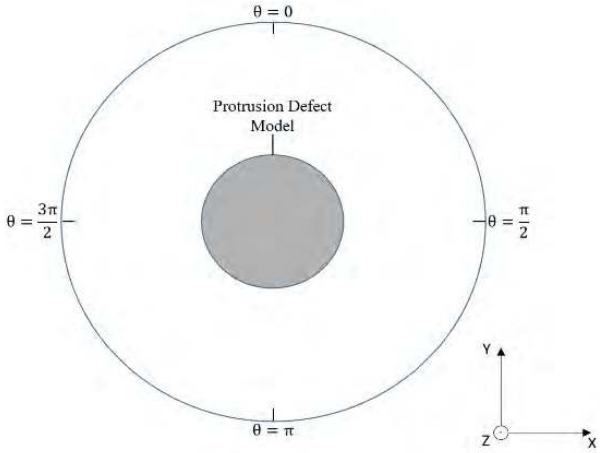

FIGURE 5. 2-D Cross-Section of a GIS Model with Protrusion Defect.

of the biggest obstacles to such propagating waves is the L-structure. Such discontinuities disturb the phases of the EM waves causing mode transformations under some circumstances. Different modes of EM waves experience the following transformation [44], [45]:

- If the input mode of propagation is TEM, Transverse Electric (TE21) will be created at the second port after the L-section (weakly since most of TEM mode maintain its shape).
- If TE11 is the input, most of the signal will be reflected back in the case of horizontal excitation, and TE21 will be obtained at the output in the case of vertical excitation.
- If TE21 is at the input port, TE11 is obtained at the output.

On the contrary, it has been shown in [46] that the TEM mode experiences no conversion. This is attributed to the fact that such waves are handled by the 'distributed constant circuit', and thus, no conversion takes place. At the point of the L-intersection, an infinite number of modes will be generated. However, after few wavelengths, the low frequency components retain their original characteristics. An increase in the peak electric field intensity might be experienced before the L-intersection because of the multiple reflections created by the discontinuity [46].

The impact of the L-section on the high frequency components of EM waves has been investigated by building a 252kV GIS model, and studying the effect of the L intersection on the electric field propagating in different directions [47]. The PD is excited along the radial direction, and hence, the electric field intensity is maximum along that direction. After the L structure, the field experience great attenuation due to the reflections of the TE components. Along the longitudinal direction, TM mode of propagation is detected. The L discontinuity acts as a source of TM mode allowing it to propagate to the second part of the tank since such mode allows the electric field to propagate in the longitudinal direction [48]. Some experimental works that were recently conducted, verified that the TM mode components of the EM wave propagates

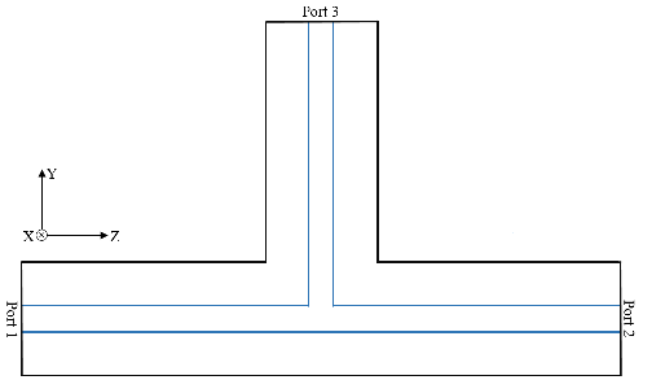

FIGURE 6. A Simplified T-Shaped Gas Insulated Switchgear Model.

after the L-intersection whether disconnecting switches are kept open or closed [49].

Finally, the effect of the L-section on the TEM and TE modes has been investigated to observe the impact of the L-structure on the low frequency and high frequency components separately [50]. Again, the TEM mode is not largely affected by the L-intersection whereas most of the reflections are attributed to the TE11 mode of propagation. Moreover, the work also shows that the peak voltage right before the L-section is higher compared to the case of straight GIS tank. This is attributed to superimposition of the reflected components of the TE11 on the incoming signals due to PD which increases the field intensity, and thus, the detected voltage [50].

C. T-SHAPED STRUCTURE

The need to study the EM waves under the influence of T-structure is essential since such structures are commonly found in GIS devices. An extensive study on the effect of T-structures on the low and high frequency components of the signal propagation were carried out in [51]. The EM wave behavior due to PD inside T-tanks depend on the port at which the PD was generated. Fig. 6 shows a simplified T-shaped GIS model. If the PD is generated at port 1, the high frequency components of the detected signals at port 2 is higher than that at port 3. The experimental results show that the transmission rate of the high frequency EM waves is about 20-30% at port 3 and about 40-50% at port 2 relative to port 1. On the contrary, the TEM mode components propagate based on the distributed constant circuit. It has been experimentally shown that the transmission rate at both ports is about 60%. The transmission rate was computed based on the distributed circuit theory, and 66.67% of the signal was supposed to be transmitted, which is slightly higher than the measured value since attenuation is not considered in the theoretical calculations [51]. If the PD is generated at port 3, the signal would be divided equally between the other 2 ports [52].

Moreover, the propagation behavior of EM waves in the x, y, and z directions shown in Fig. 6 is investigated to provide better understanding of the EM signal propagation [53]. A protrusion defect is modeled as a small needle placed along

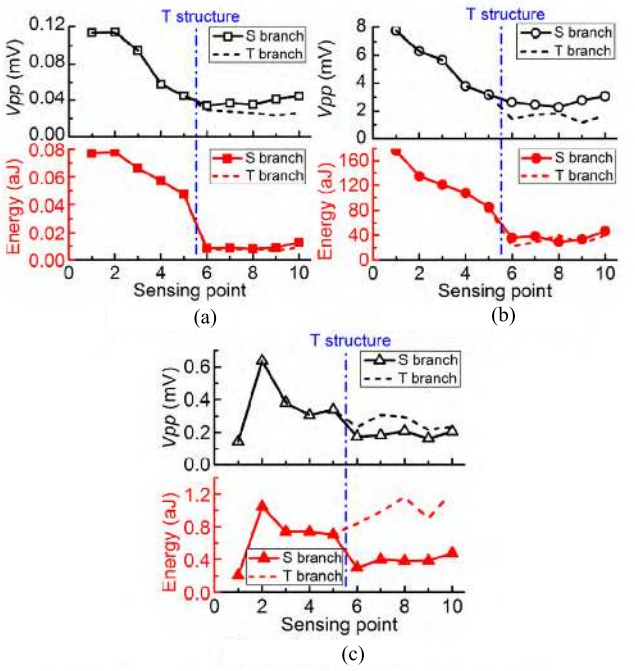

FIGURE 7. Attenuation curves for peak voltages and Energy $\theta = 0°$ [54].

the y-axis close to port 1, and a pulse is applied to the needle. The electric field intensity is dominant in the y-direction, and results show that the straight section (SS) has greater intensity compared with the T-section (TS). Moreover, the field intensity in the x-direction is very small. The relative angle effect is also studied by investigating the propagation characteristic of EM waves inside a T-shaped GIS in different circumferential angles using FDTD [54]. Fig. 7 and Fig. 8 summarizes the attenuation characteristics measured at two different circumferential angles for both Straight-section (S) and the T-branch (T). Ten equally spaced probes were modelled to measure the voltage intensity due to the EM waves. Five out of which are placed before the T-structure. As shown in Fig. 7 and Fig. 8, the dominant direction is always the radial direction, and the T-branch energy is always higher than that of the straight branch along the z-direction since the discontinuity acts as a source to the TM mode.

The time of flight through a T-structure is largely dependent on the PD source location relative to the inner or outer conductor [55]. To illustrate, if the PD source is close to the outer tank, results might not be very accurate compared with the theoretical calculations of the time of flight. This is attributed to the fact that a different path for the wave will be taken if the PD source is generated close to the outer tank. Finally, mode transformation also takes place in T-structures since higher order modes are also created at the discontinuity [56]–[58]. The following rules are obtained for the case where PD source is generated at port 1 (refer to Fig. 6):

- If the input is TEM mode, the output at ports 2 and 3 is TE21.
- TE11 transforms to TE21.

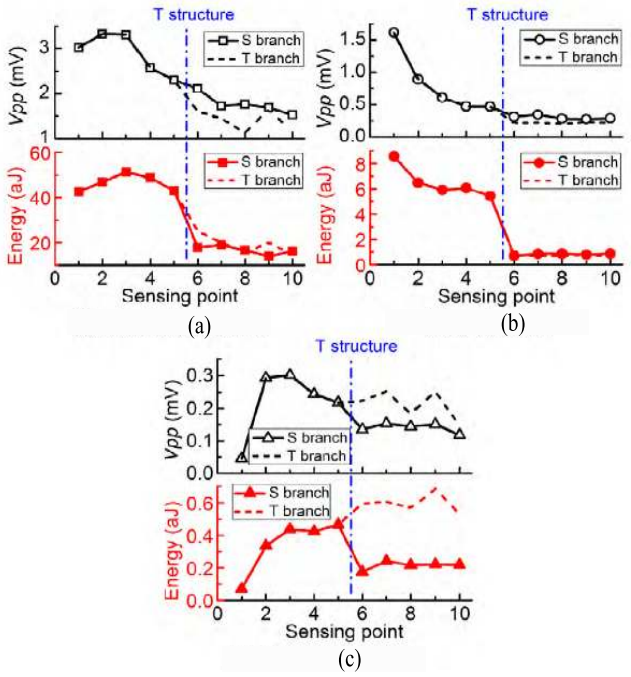

FIGURE 8. Attenuation curves for peak voltages and Energy at $\theta = 90°$ [54].

- TE21 retains its mode at both ports if the excitation is in the 45° direction. Otherwise, TE21 changes to TE11 at port 3.

If port 3 is the input of the PD source, similar mode transformation will be obtained at port 1 and port 2. S. Okabe *et al*. [59] modeled a T-section GIS and applied a protrusion defect at port 3 shown in Fig. 6. The following are obtained (holds under the assumption that the cutoff frequency includes TE21 modes):

- If TEM mode is at the input, TE21 (0 degree) will be the dominant mode at the outputs.
- If TE11 (0 degree) is at the input, it will mostly retain its mode at the outputs.
- If TE11 (90 degrees) is at the input, TE21 (45 degrees) will be the dominant mode at the outputs.

D. DISCONNECTING PARTS AND CHANGE OF RADII RATIO

Circuit breakers, switches (disconnectors), and isolators are some of the common components that are comprised in GIS tanks. Such components can affect the propagation of EM waves. A GIS in the simplest form can be thought of as a coaxial cable which supports TEM and other higher order modes [60], [61]. Nevertheless, if a disconnecting component of the GIS is opened for any reason, propagating EM waves can no longer see the GIS as a coaxial cable but rather, it is seen as a circular waveguide (CW). CW cannot support TEM mode of propagation since they are made of a single conducting material, and thus, potential difference between 2 conductors cannot be achieved to get the TEM mode [60].

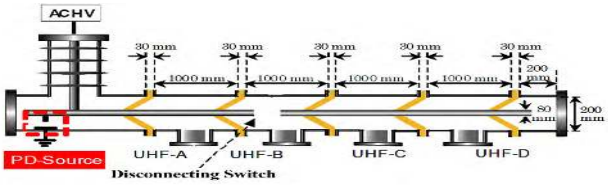

FIGURE 9. Gas Insulated Switchgear Model with a Disconnecting Switch Being Open [64].

Solving the Helmholtz equation for E-field, the following two equations for TEM and TE modes are obtained:

$$\frac{1}{r}\frac{\partial}{\partial r}\left(r\frac{\partial V}{\partial r}\right)+\frac{1}{r^2}\frac{\partial^2 V}{\partial \phi^2}=0 \quad (For\ TEM) \tag{11}$$

$$\frac{1}{r}\frac{\partial}{\partial r}\left(r\frac{\partial V}{\partial r}\right)+\frac{1}{r^2}\frac{\partial^2 V}{\partial \phi^2}+\frac{\partial^2 V}{\partial z^2}=-k^2V \quad (For\ TE) \tag{12}$$

where r, ϕ, and z are the coordinates of the cylindrical system, V is potential function, and k is the propagation constant. It can be seen that the TEM mode does not have a longitudinal component (z-direction), and the velocity of the wave is not frequency dependent. On the contrary, TE (and TM) mode has cutoff frequencies below which waves cannot propagate [62]. The cutoff frequencies for the TE and TM modes of coaxial waveguides are calculated using the following equations [63]:

$$f_{cTEm1}=\frac{c\cdot m}{\pi(a+b)} \tag{13}$$

$$f_{cTM1n}=\frac{c\cdot n}{2(b-a)} \tag{14}$$

where a and b are the inner and outer radii of the coaxial cable respectively, and m and n are integers to determine the mode of operation for the TE and TM modes respectively.

To understand the effect of opening a disconnecting switch inside the GIS tank, a FDTD model for a GIS with SF6 gas being in series with the high voltage conductor as shown in Fig. 9 is built [64]. Both high frequency (HF) and low frequency (LF) components were measured and simulated separately through the use of filters. The couplers connected after the switch (UHF B, C, and D) could not detect most of the LF (TEM) components of the electromagnetic waves. The EM waves can no longer see the GIS in this case as a coaxial cable, but rather a CW which does not support TEM mode of propagation [64], [65]. In addition, results show that if the gap length is increased, more TEM frequency components would be attenuated resulting in higher energy losses. High frequency components (TE11 mode and above) on the other hand do not experience large attenuation in the magnitude since they can freely propagate in circular waveguides.

The effect of disconnecting switches was further studied in [63]. This is done by investigating the impact of the switch for three different classes of GIS (110kV, 220 kV, and 550kV). It has been shown that the higher the voltage (or the larger the GIS dimensions), the lower the attenuation of EM waves due to a disconnecting switch. This could be justified by the fact that the larger the dimensions of the GIS, the lower the cutoff frequency of the first propagating mode, the lower

the TEM content, the lower the reflections due to the low order modes.

The impact of changing the diameter ratio between the inner and outer conductors was also investigated in [63]. The work has shown that EM wave energy is attenuated after the change in inner radius. Such results are expected since changing the ratio between the inner and outer conductor radii changes the characteristic impedance of coaxial waveguide. The characteristic impedance of a lossless line is given by [66]:

$$Z_0 = \frac{60}{\sqrt{\epsilon_r}} ln\left(\frac{a}{b}\right) \tag{15}$$

where a and b are the inner and outer radii of the coaxial cable respectively.

Further investigation on the change of outer diameter was carried out in [67]. The results showed that the TEM mode of propagation experiences a minute impact due to a change in diameter whereas the higher order modes are largely reflected back.

E. INSULATING SPACERS

Dielectric spacers are solid insulating components used to separate GIS compartments and provide better support between inner and outer conductors [68], [69]. However, such components enforce some constraints on the highest possible applied voltage between the two conductors of GIS at the interfaces between the solid, gas, and electrode interface [70]. Many attempts have been proposed to optimize the shape of dielectric spacers to reduce the electric field stress and thus, increase the breakdown voltage of GIS. Consequently, different types of insulations are proposed including but not limited to disk-type, cone-type, and basin-type spacers [68], [71].

To understand the impact of dielectric spacers on the EM waves generated in the event of a fault, an experimental investigation to study and analyze the intensity of the detected field after passing through basin-type insulators was carried out in [11], [72]. FDTD modeling was also used to further investigate the effects of spacers. Two types of basin-type spacers were used to analyze the impact on the EM waves. As depicted in Fig. 10, the metal type has a metallic cover surrounding the spacer to reduce the electric field leakage and provide better grounding for the tank, whereas the bush type does not have any metal cladding.

The main factor that contributes to EM attenuation is not the permittivity difference between SF6 and the dielectric spacer. This has been investigated by initially applying low pass filtering to the EM wave to inspect the attenuation of the TEM mode of propagation [11], [72]. The obtained results showed that the low frequency components experienced very small attenuation in the amplitude as the signal propagate through the spacers. When high pass filtering is applied to the obtained EM waves, the higher order modes of propagation experienced large attenuation. As the EM wave propagate inside the tank, higher order modes start to get decomposed since different modes of propagation have different velocities

(a) (b)

FIGURE 10. Basin-Type Insulating Spacers [11]. (a) Bush type (BT). (b) Metal flange type (MT).

at which they travel. Hence, reduction in the amplitude of the signal is experienced even in the absence of dielectric spacers [72].

A simulation model has been built to investigate the effect of the spacers on the time of flight of EM waves [73]. The results of the simulation model showed that EM waves cannot propagate at the speed of light with the existent of spacers. The speed of propagation is inversely proportional to the square root of the relative dielectric constant [52]. Thus, the propagation with the existence of dielectric spacers with high relative permittivity would be slower than the speed of light. The results of the work also showed that the EM waves traveled through the path with the minimal resistance. Thus, thickness of spacers is the main factor that affect the velocity of the EM waves rather than their shape.

Table 1 below summarizes the impact of the different discontinuities in GIS devices discussed in section 4.

V. UHF SENSOR CONNECTION

A. EXTERNALLY CONNECTED UHF SENSORS

Albeit internally connected UHF sensors demonstrate superior performance compared with the externally connected counterparts in both noise and sensitivity, the later has been given great attention lately due to the many challenges associated with the connection of internal sensors in already built GIS devices. This could be attributed to the fact that GIS is a concealed device which imposes high cost and time for the integration of sensors internally [74].

For bush type Spacers, EM waves can easily leave the tank through the dielectric spacer [9]. S. Kaneko *et al*. [75] built a FDTD model for a GIS with slits formed by the bolts connecting the GIS tubes together. For the induced EM wave, the slits act as slot antennas with width equal to the thickness of the spacer and length equal to the spacing between 2 adjacent bolts. This gives the externally connected sensors an advantage if the measured frequency of the PD event is close to the resonance frequencies of the slot antennas [74], [76]. The detected electric field intensity is maximum if the UHF is connected in the middle between 2 adjacent bolts [74], [75]. In order for the electric field vector to meet the boundary conditions at the aperture, the field lines have to be in the longitudinal direction parallel to the GIS tank. Thus, when con-

TABLE 1. Discontinuity types and their impact on the EM wave propagation.

Discontinuity Type	Impact
Angle Between PD Source and Sensor	• If the angle between the PD source and the used coupler is 0°, the detection intensity is maximum. If the angle is 90°, the detection intensity is minimal. If the angle is 180°, the behavior is similar to the 0°, but slightly lower than that at 0° since the inner conductor create a discontinuity for the waves causing some reflections [41] – [44].
L-Section T-Section	• Signal transformation takes place at the L-structures as well as T-structures [45], [58]. • Low frequency components are mostly transmitted through the L-structure to the other port whereas most of the TE11 mode is reflected back. On the other hand, the L-structure acts as a source to the TM mode of propagation allowing it to propagate to the other port [47], [48]. • For T-structure, if port 3 (refer to Fig. 6) is the port at which PD occurred, the signals will be divided equally between the other 2 ports with similar behaviour. If port 1 (port 2) is the source of PD activity, high frequency components will be greater at port 2 (port 1). On the other hand, the low frequency components propagate based on the distributed circuit component [52] – [55].
Disconnecting Parts and Change of Radius Ratio	• Disconnecting switches change the waveguide type from coaxial waveguide to CW which does not support TEM Mode of propagation. Thus, low frequency components are attenuated [65]. • Increasing (decreasing) the inner or outer radius of the GIS would result in multiple wave reflections [64].
Spacers	• Spacers have a minute impact on the reflection of EM waves [11]. • The time of flight on the other hand can be largely affected by spacers. That is, EM wave velocity is dependent on the number of spacers and the corresponding thickness [74].

necting an external antenna to detect the produced EM waves due to PD, the E-plane of the sensor has to be fixed parallel to the GIS tank to maximize the sensitivity of the detected field [39], [74].

Different kinds of external sensors are used to detect the event of PD. The most commonly used types of external sensors are the bi-conical log periodic antenna, Horn antenna, loop antenna, dipole antenna, and some kinds of planar antennas including Fractal antenna, patch antenna (asymmetric and symmetric), and Spiral antenna [9], [39], [74], [77], [78]. Horn antennas have higher sensitivity at high frequencies whereas log-periodic antennas have better sensitivity at low frequencies. The loop antenna has better sensitivity at the higher frequency side of the spectrum. One of the factors that makes such antenna superior compared with the other two aforementioned types is that the position of the loop antenna does not have to be exactly in the middle between bolts to get good sensitivities. The dipole antenna, conversely, has the best sensitivity as it can be directly connected to the flanges measuring both field intensity and potential difference between the 2 flanges in the event of PD [74]. Microstrip patch antennas are small, narrow bandwidth, and cheap devices printed into a circuit board, and made with a conductive material such as copper [79], [80]. A spiral antenna is a wideband circularly polarized type of antenna with a relatively low gain [81], [82]. Fractal antennas are small, multiband, broad bandwidth antennas. Although Hilbert fractal antenna is the most commonly used type of such antennas, there are also some other types like the Moore fractal antenna [77], [83], [84].

B. INTERNALLY CONNECTED UHF SENSORS

Recently, GIS devices are built with UHF sensors integrated internally to detect PD properly. Such sensors are usually connected in the hand-hole of GIS tanks. Consequently, there are restrictions on the maximum size of the internally connected antennas. Another drawback of the use of such devices is that it affects the electric field distribution inside the GIS enclosure [85], [86]. Moreover, if maintenance is required for one of the UHF sensors in the event of failure, changing internally connected sensors or fixing them requires more effort and time [9].

The position of the PD source can affect the behavior of the detected electric field by sensors. To illustrate, if the PD source is close to the inner conductor, the TE11 mode of propagation is dominant and thus, the detected EM wave would have a short duration. On the contrary, if the defect was on the outer tank, higher order TE modes would be generated increasing the duration of the detected signals [87], [88]. The increase in duration is caused by the reduction in the velocity of the higher order modes of propagation which is given by the following equation for the TE modes:

$$v_{TE} = v.\sqrt{1 - \left(\frac{f_c}{f}\right)^2} \tag{16}$$

where f_c is the cutoff frequency of the TE mode, v is the propagation velocity, and f is the operating frequency. One important point to note is that if the GIS size is small, it might be difficult to differentiate whether PD source is on the low or the high voltage conductor [87]. When the GIS size is small, the tip of the needle used to create the protrusion defect would be close to both the inner and outer conductors making it hard to determine whether the needle is on the inner or outer conductor.

Table 2 summarizes some of the important electromagnetic aspects investigated by researchers in the event of PD in GIS.

Due to the size constraint imposed on the internally connected UHF sensors, limited types of such devices could be used to detect PD. Disk-type and loop-type sensors are the most well-known sensors used for this purpose. The performance of the two types of UHF couplers, or antennas

TABLE 2. Comparison between Different Methods for EM Behaviour in Gas Insulated Switchgears.

Ref.	Main Discontinuity Type	Sensor	Covered Frequency Band	Remarks
[9] [39]	No Discontinuities	Fat Dipole (Dissymmetric) Antenna Connected Externally	0.5GHz – 3GHz	• Two types of excitations were used to model the PD accurately. Linefeed to model the TEM mode and waveguide feed to model the higher order modes. • With the use of external sensors, the cut off frequency of leaked signal is determined by rectangular waveguides. • Linear antennas placed along the axis which is parallel to the GIS is the optimal way for maximum detection efficiency.
[11] [72]	Basin-Type Spacers	- Disk Type UHF Sensors - Horn Antenna Connected Externally	Time Domain Results only	• The obtained results show that the transmission rate percentage inside the GIS is always higher when using the metal type insulating spacer if the same fault type is applied. • The use of internal and external sensors gave similar behavior with the exception that the detected field intensity is larger with internal sensors.
[22]	L-Section and T-Section	Disk-Type UHF Sensors	0-3GHz	• A Finite Element (FE) model that assumes perfect conductors and a non-dispersive insulating spacers is built in this work. • The results show that coupling is low at low frequencies and is high at high frequencies. This is explained by the fact that many sharp edges and resonances will be created at the high frequencies causing S-parameters to have such a behavior.
[32]	Bus Bar	Ideal Probes	0-3GHz	• A near field to far field transformation model has been built to study the EM wave propagation due to a PD. The obtained results were verified with the use of numerical solver, and results with high accuracy were obtained. • Insulation material can have a large impact on the low frequency components. • Bus-bar have a minimal effect on the EM waves because its size is much smaller than the wavelength.
[43]	No Discontinuities	Probe Coupler	0 – 3.5 GHz	• The longer the distance between the source of PD and the coupler, the weaker the detected electric field intensity due to dispersion effect. • When the angle between source and probe is 90 (Fig. 5), only even-number TE modes are detected in the frequency domain since TE odd modes have nodal points of intensity strength.
[45]	L-Section/ Spacer	Ideal Sensing Probes (Simulations only)	0.3 – 1 GHz	• As the distance between the consecutive spacers is increased, more resonances occur. • As the number of spacers is increased, more resonances takes place due to the increased reflections between the spacers. • TE11 mode causes the largest portion of reflection at the L-intersection.
[46]	L-Section	Ideal Sensing Probes (Simulations only)	0 – 2 GHz	• L-section caused a large reduction in the amplitude of the higher order modes. • L section causes mode transformation to EM waves propagating inside GISs.
[47]	L-Section	Ideal Sensing Probes	Time Domain Results only	• TM mode can pass through an L-intersection since the electric field in such mode can travel in the longitudinal direction.
[51]	T-Structure	Disk-Type Sensors	Time Domain Results only	• Low frequency components can propagate as in distributed circuit model, whereas TE modes experience reflections and attenuation. • Experiments performed in 2 different types of GISs to verify the obtained conclusions.
[53]	T-Structure	UHF Probes	-	• Most of the field along the y-direction (Fig. 6) will propagate to the SS. • Field along the x-direction is negligible. • Field along the z-direction mostly propagates along the TS (The TS could be thought of as a source to the TM mode of propagation).
[54]	T-Structure	Ideal Sensing Probes	0-3.5GHz	• The frequency domain spectrum shows peaks at cutoff frequencies corresponding to the different modes in all directions. In the x-direction and y-direction, the peaks appear at the different TE modes whereas TM mode peaks appear in the z-direction (Fig. 6).
[56]	T-Structure	Disk-Type Sensors	0.35GHz-0.75GHz	• For the case where the used cut off frequency is below the TE21 frequency bands, TE11 behaviour of T-structure is similar to that of L-structures. It should be noted that the magnitude of the transformed modes might not be the same.
[59]	T-Structure and L-Structure	UHF Sensor	-	• If TE11 was incident at an oblique angle (that is, an angle other than 0 or 90 degrees), the characteristics of the propagated field can be obtained by the superposition of the 2 aforementioned types. • Electromagnetic wave modes inside a straight GIS are preserved. Thus, one can utilize this property to distinguish between noise and generated signal due to PD inside the tank.
[63]	Disconnecting Switch and Change in Radius	- Ideal Sensing Probes - External Sensors	0-2GHz	• The effect of increasing and decreasing the inner radius of the GIS were similar as expected (refer to (15)). • The energy of the EM waves right before the change in characteristic impedance due to increasing/decreasing the radius is usually high due to the reflections at that point.

TABLE 2. ***(Continued.)*** **Comparison between Different Methods for EM Behaviour in Gas Insulated Switchgears.**

Ref.	Main Discontinuity Type	Sensor	Covered Frequency Band	Remarks
[64]	Disconnecting Switch	Disk-Type UHF Sensors	0-8GHz	• When disconnecting switches are open, multiple reflections on the EM waves could occur causing the peak voltage to increase before the switch (Sensor A in Fig. 9).
[74]	Spacers	- Horn Antenna - Dipole Antenna - Loop Antenna - Log-Periodic Antenna	0-3GHz	• The proposed improved dipole antenna showed superior sensitivity for voltage detection (2 times larger than the horn antenna). This could be attributed to the fact that the proposed sensor was directly measuring the potential between the 2 tubes connected via the spacer. • Noise issue could be reduced if the measured frequency band is limited to a relatively narrow band which contain the resonance frequency of the slot antenna(s).
[75]	Spacers	-	0-1.2GHz	• As the number of bolts used to connect GIS tubes increases, the number of slots also increase, increasing the resonance frequency. • Increasing the width of the slots increase the bandwidth of the antenna. • As the dielectric constant increases, the resonant frequency decreases.
[77]	-	- Moore Fractal Antenna - Hilbert Fractal Antenna	0-3GHz	• Both Hilbert and Moore fractal antennas have high directivity. • Moore fractal antenna has higher sensitivity and better waves reception compared with the Hilbert counterpart.
[84]	-	- Stacked Hilbert Antenna - Hilbert Antenna	0-1GHz	• Stacked Hilbert antenna has superior performance compared with the conventional Hilbert antenna in gain and Bandwidth. • The stacked Hilbert antenna has 2 parasitic Hilbert curves where one end is directly connected to the original Hilbert conductor and the other end is left as open circuit.
[85]	-	Asymmetrical Octagonal Monopole Antenna	0-3GHz	• The impedance matching of the proposed antenna is improved by shifting the symmetrical conventional antenna into an asymmetrical one. • Size reduction is achieved by cutting the edge of the antenna. • More resonances were obtained by etching the ground plane into ɼ shape.
[87]	-	- Patch Antenna - Log Periodic Antenna - Waveguide Slot Antenna	0-2GHz	• The larger the antenna size, the better the sensitivity of detection. Consequently, the waveguide slot antenna showed the best measured results of the three antenna types used.
[88]	-	- Disk-Type Antenna - Loop-Type Antenna	0-8GHz	• Loop-type antennas are usually embedded in the insulator when used for detection of PD in GISs. • Disk-type antennas are connected internally, but close to the outer tank wall as shown in Fig. 9.
[91] [92]	Spacer (Not main but is used)	Disk Couplers	0-6GHz	• Three different types of defects were simulated namely a metal particle attached to the central conductor, a particle attached to the outer conductor, and a particle attached to the insulator. • E-Field intensity was measured internally and externally to understand the EM wave propagation behavior. Propagation was verified to be in the longitudinal direction. • Low frequency components cannot leave the GIS tank making it hard to detect such fields externally.

were investigated [88]. The results showed that disk-type has better sensitivity for the detection of higher order modes. Thus, if PD took place near the outer tank, disk-type sensors demonstrate superior capabilities. The loop-type antennas on the other hand are good at lower frequencies which make them good candidates if PD occurred near the central conductor. Disk-type antennas can either be connected internally or externally [85], [88]–[90]. Extensive research has been carried out to improve the performance of disk-type antennas used for the detection of UHF signals. To summarize, internally and externally connected sensors deliver similar behavior for the detection of PD [11]. However, the internally connected sensors have much higher sensitivities compared with the external counterparts.

VI. CONCLUSION

Gas Insulated Switchgears have become essential components in the power system utilities due to their higher efficiency, reliability, and smaller size. With the rapid technological growth in the field of power systems, the need for continuously monitor such devices has become of great importance. UHF method for the diagnostic of GIS has become widely used due to the many benefits including but not limited to high sensitivity and large immunity to noise and interferences. Thus, this paper is meant to discuss the EM wave behavior due to PD detected by the UHF techniques in GIS devices. The main concluding remarks are:

- There are two types of mechanisms that govern the phenomenon of PD namely Townsend and Streamer

mechanisms. If the void or gap size is small, Townsend mechanism explains the behavior of PD. Nevertheless, if the gap size gets larger, Streamer mechanism explains the space charge and formulation of photons.
- Different types of pulse models can be used to represent the PD pulse. Such models include Gaussian pulse, Wanninger pulse, and Double Exponential pulse.
- The Larmor's formula explains the radiation of the electromagnetic waves during the event of PD which is caused by the acceleration and deceleration of charged particles.
- The EM radiation due to small voids or gaps can be modelled as an electric dipole.
- The angle between the PD source and the coupler used to detect EM waves has a large impact on the intensity of the detected signals.
- L and T-structures can cause mode transformation to the signal propagation. Such structures can also cause large attenuation to EM waves.
- Disconnecting switches can change the environment of the GIS from coaxial waveguide to circular waveguide causing attenuation to the TEM mode components.
- Changing the inner or outer radii of GISs can cause reflections in the EM waves.
- Spacers do not have a large impact on the attenuation of the EM waves, but they can affect the time of flight of waves.
- Internally connected sensors have better sensitivity than the external sensors since the later receive weaker signals and are more prone to noise.

ACKNOWLEDGMENT

This publication was made possible by NPRP [10-0101-170085] from the Qatar National Research Fund (a member of the Qatar Foundation). The statements made herein are solely the responsibility of the authors.

REFERENCES

[1] M. D. Judd, L. Yang, and I. B. B. Hunter, "Partial discharge monitoring of power transformers using UHF sensors. Part I: Sensors and signal interpretation," *IEEE Elect. Insul. Mag.*, vol. 21, no. 2, pp. 5–14, Mar./Apr. 2005.
[2] M.-X. Zhu, Q. Liu, Y.-B. Wang, Y. Li, J.-B. Deng, H.-B. Mu, and G.-J. Zhang, "Optimisation of antenna array allocation for partial discharge localisation in air-insulated substation," *IET Sci., Meas. Technol.*, vol. 11, no. 8, pp. 967–975, Nov. 2017.
[3] S. Masuda, T. Koga, M. Kozako, M. Hikita, H. Haruyama, I. Kato, H. Sato, and F. Aono, "Basic study on measurement of electromagnetic waves emitted by partial discharge in cable joint for high voltage overhead transmission" in *Proc. Int. Symp. Elect. Insul. Mater. (ISEIM)*, Toyohashi, Japan, Sep. 2017, pp. 547–550.
[4] G. C. Stone, E. A. Boulter, I. Culbert, and H. Dhirani, *Electrical Insulation for Rotating Machines: Design, Evaluation, Aging, Testing, and Repair*. Piscataway, NJ, USA: IEEE, 2004.
[5] H. H. Sinaga, "Detection identification and localization of partial discharges in power transformers using UHF techniques," Ph.D. dissertation, Dept. School Elect. Eng. Telecommun., Univ. New South Wales, Sydney, NSW, Australia, Mar. 2012.
[6] D. Dai, X. Wang, J. Long, M. Tian, G. Zhu, and J. Zhang, "Feature extraction of GIS partial discharge signal based on S-transform and singular value decomposition," *IET Sci., Meas. Technol.*, vol. 11, no. 2, pp. 186–193, Mar. 2017.
[7] S. Meijer, "Partial discharge diagnosis of high-voltage gas-insulated systems," Ph.D. dissertation, Delft Univ., Delft, The Netherlands, Nov. 2001.
[8] X. Fan, L. Li, Y. Zhou, N. Tang, Z. Zou, X. Li, G. Huang, and M. Liu, "Online detection technology for SF_6 decomposition products in electrical equipment: A review," *IET Sci., Meas. Technol.*, vol. 12, no. 6, pp. 707–711, Sep. 2018.
[9] H. Guo, F. Lu, and K. F. Ren, "Simulation and measurement of PD-induced electromagnetic wave leakage in GIS with metal belt," *IEEE Trans. Dielectr. Electr. Insul.*, vol. 21, no. 4, pp. 1942–1949, Aug. 2014.
[10] X. Li, X. Wang, A. Yang, D. Xie, D. Ding, and M. Rong, "Propogation characteristics of PD-induced UHF signal in 126 kV GIS with three-phase construction based on time–frequency analysis," *IET Sci., Meas. Technol.*, vol. 10, no. 7, pp. 805–812, Oct. 2016.
[11] M. Hikita, S. Ohtsuka, G. Ueta, S. Okabe, T. Hoshino, and S. Maruyama, "Influence of insulating spacer type on propagation properties of PD-induced electromagnetic wave in GIS," *IEEE Trans. Dielectr. Electr. Insul.*, vol. 17, no. 5, pp. 1642–1648, Oct. 2010.
[12] A. Sabot, A. Petit, and J. P. Taillebois, "GIS insulation co-ordination: On-site tests and dielectric diagnostic techniques. A utility point of view," *IEEE Trans. Power Del.*, vol. 11, no. 3, pp. 1309–1316, Jul. 1996.
[13] Y. Wang, J. Li, H. Liang, H. Yu, and X. Zhao, "Characteristic analysis of partial discharge detection in GIS," *Int. J. Digit. Content Technol. Appl.*, vol. 6, no. 18, p. 482, 2012.
[14] W. Gao, D. Ding, W. Liu, and X. Huang, "Analysis of the intrinsic characteristics of the partial discharge induced by typical defects in GIS," *IEEE Trans. Dielectr. Electr. Insul.*, vol. 20, no. 3, pp. 782–790, Jun. 2013.
[15] S. S. Refaat and M. A. Shams, "A review of partial discharge detection, diagnosis techniques in high voltage power cables," in *Proc. IEEE 12th Int. Conf. Compat., Power Electron. Power Eng.*, Doha, Qatar, Apr. 2018, pp. 1–5.
[16] R. Bartnikas, "Partial discharges. Their mechanism, detection and measurement," *IEEE Trans. Dielectr. Electr. Insul.*, vol. 9, no. 5, pp. 763–808, Oct. 2002.
[17] M. M. Yaacob, M. A. Alsaedi, J. R. Rashed, A. M. Dakhil, and S. F. Atyah, "Review on partial discharge detection techniques related to high voltage power equipment using different sensors," *Photon. Sensors*, vol. 4, no. 4, pp. 325–337, Dec. 2014.
[18] B. Qi, C. Li, Z. Hao, B. Geng, D. Xu, S. Liu, and C. Deng, "Partial discharge detection for GIS: A comparison between UHF and acoustic methods," in *Proc. IEEE Int. Symp. Electr. Insul.*, Jun. 2010, pp. 1–5.
[19] M. Ren, J. Zhou, S. Yang, T. Zhuang, M. Dong, and R. Albarracín, "Optical partial discharge diagnosis in SF_6 gas-insulated system with SiPM-based sensor array," *IEEE Sensors J.*, vol. 18, no. 13, pp. 5532–5540, Jul. 2018.
[20] F. Álvarez, F. Garnacho, J. Ortego, and M. Á. Sánchez-Urán, "Application of HFCT and UHF sensors in on-line partial discharge measurements for insulation diagnosis of high voltage equipment," *Sensors*, vol. 15, no. 4, pp. 7360–7387, Apr. 2015. doi: 10.3390/s150407360.
[21] E. Jennings and A. Collinson, "A partial discharge monitor for the measurement of partial discharges in a high voltage plant by the transient earth voltage technique," in *Proc. Int. Conf. Partial Discharge*, Sep. 1993, pp. 90–91.
[22] G. Behrmann and J. Smajic, "RF PD signal propagation in GIS: Comparing S-parameter measurements with an RF transmission model for a short section of GIS," *IEEE Trans. Dielectr. Electr. Insul.*, vol. 23, no. 3, pp. 1331–1337, Jun. 2016.
[23] M. Wu, H. Cao, J. Cao, H.-L. Nguyen, J. B. Gomes, and S. P. Krishnaswamy, "An overview of state-of-the-art partial discharge analysis techniques for condition monitoring," *IEEE Elect. Insul. Mag.*, vol. 31, no. 6, pp. 22–35, Nov./Dec. 2015.
[24] Solanki. (2017). *Breakdown in Gases*. Accessed: Sep. 19, 2018. [Online]. Available: https://www.slideshare.net/nirajsolanki33/breakdown-in-gases
[25] K. Korneliussen, "Partial discharges and breakdown voltage in designs with triple junctions under AC stress," M.S. thesis, Norwegian Univ. Sci. Technol., Trondheim, Norway, 2016.
[26] M. Abdel-salam, H. Anis, A. El-Morshedy, and R. Radwan, *High Voltage Engineering: Theory and Practice*, 2nd ed. New York, NY, USA: Marcel Dekker, 2000.
[27] Almatri. (2015). *Streamer Theory*. Accessed: Sep. 19, 2018. [Online]. Available: https://www.slideshare.net/mohammedalmatri7/streamer-theory
[28] A. Pedersen, T. Christen, A. Blaszczyk, and H. Boehme, "Streamer inception and propagation models for designing air insulated power devices," in *Proc. IEEE Conf. Elect. Insul. Dielectric Phenomena*, Oct. 2009, pp. 604–607.
[29] J. Dengwei, "Frequency spectrum properties and propagation features of typical PD in the GIS," High Voltage Test Syst., Shanghai, China, Tech. Rep., Aug. 2016. [Online]. Available: https://himalayal.com

[30] M. D. Judd and O. Farish, "High bandwidth measurement of partial discharge current pulses," in *Proc. IEEE Int. Symp. Elect. Insul.*, vol. 2, Jun. 1998, pp. 436–439.
[31] A. J. Reid and M. D. Judd, "High bandwidth measurement of partial discharge pulses in SF6," in *Proc. 14th Int. Symp. High Voltage Eng.*, Beijing, China, Aug. 2005, pp. 1–6.
[32] Y. Qi, Y. Fan, B. Gao, Y. Mengzhuo, A. Jadoon, Y. Peng, and T. Jie, "Study on the propagation characteristics of partial discharge in switchgear based on near-field to far-field transformation," *Energies*, vol. 11, no. 7, p. 1619, 2018.
[33] M. Sadiku, *Elements of Electromagnetics*. New York NY, USA: Oxford Univ., 2007.
[34] C. A. Balanis, *Antenna Theory: Analysis and Design*. Hoboken, NJ, USA: Wiley, 2016.
[35] K. Lonngren and S. Savov, *Fundamentals of Electromagnetics With MATLAB*, 1st ed. Rijeka, Croatia: SciTech, 2005.
[36] T. Johnson, "Class lecture, topic: The larmor formula," School Eng. Sci., KTH Roy. Inst. Technol. Stockholm, Stockholm, Sweden, Lecture 12, Feb. 2017.
[37] Y. Shibuya, S. Matsumoto, M. Tanaka, H. Muto, and Y. Kaneda, "Electromagnetic waves from partial discharges and their detection using patch antenna," *IEEE Trans. Dielectr. Electr. Insul.*, vol. 17, no. 3, pp. 862–871, Jun. 2010.
[38] J. S. Stratton, *Electromagnetic Theory*. Hoboken, NJ, USA: Wiley, 2007.
[39] H. Guo, H. Qiu, L. Yao, F. Huang, and K. F. Ren, "Investigation on polarization characteristics of PD-induced electromagnetic wave leakage in GIS with metal belt," *IEEE Trans. Dielectr. Electr. Insul.*, vol. 23, no. 3, pp. 1475–1481, Jun. 2016.
[40] M. D. Judd, O. Farish, and B. F. Hampton, "The excitation of UHF signals by partial discharges in GIS," *IEEE Trans. Dielectr. Electr. Insul.*, vol. 3, no. 2, pp. 213–228, Apr. 1996.
[41] T. Li, J. Pan, X. Li, X. Pang, C. Gu, M. Rong, and X. Wang, "The optimal circumferential angle position of UHF sensor for partial discharge detection in GIS," in *Proc. IEEE Int. Conf. High Voltage Eng. Appl. (ICHVE)*, Chengdu, China, Sep. 2016, pp. 1–4.
[42] Sriyono, W. A. Putro, K. Nishigouchi, U. Khayam, Suwarno, M. Kozako, M. Hikita, K. Urano, and C. Min, "Sensitivity verification and determination of the best location of external UHF sensors for PD measurement in GIS," in *Proc. IEEE Int. Conf. Condition Monit. Diagnosis*, Bali, Indonesia, Sep. 2012, pp. 698–701.
[43] T. Li, X. Wang, C. Zheng, D. Liu, and M. Rong, "Investigation on the placement effect of UHF sensor and propagation characteristics of PD-induced electromagnetic wave in GIS based on FDTD method," *IEEE Trans. Dielectr. Electr. Insul.*, vol. 21, no. 3, pp. 1015–1025, Jun. 2014.
[44] H. Muto, M. Yoshimura, C. Nishida, S. Okabe, and S. Yuasa, "Simulation of propagation characteristics of higher order mode electromagnetic waves in GIS," in *Proc. 7th Int. Conf. Properties Appl. Dielectr. Mater.*, Nagoya, Japan, vol. 1, Jun. 2003, pp. 227–231.
[45] S. Okabe, H. Muto, M. Yoshimura, C. Nishida, and S. Yuasa, "Simulation of propagation characteristics of higher order mode electromagnetic waves in GIS," *IEEE Trans. Dielectr. Electr. Insul.*, vol. 13, no. 4, pp. 855–861, Aug. 2006.
[46] M. Hikita, S. Ohtsuka, T. Teshima, S. Okabe, and S. Kaneko, "Examination of electromagnetic mode propagation characteristics in straight and L-section GIS model using FD-TD analysis," *IEEE Trans. Dielectr. Electr. Insul.*, vol. 14, no. 6, pp. 1477–1483, Dec. 2007.
[47] X. Wang, T. Li, D. Ding, and M. Rong, "The influence of L-shaped structure on partial discharge radiated electromagnetic wave propagation in GIS," *IEEE Trans. Plasma Sci.*, vol. 42, no. 10, pp. 2536–2537, Oct. 2014.
[48] T. Li, M. Rong, D. Liu, and X. Wang, "Study on propagation characteristics of partial discharge-induced UHF signal in GIS with L shaped structure," in *Proc. 2nd Int. Conf. Electr. Power Equip.-Switching Technol. (ICEPE-ST)*, Oct. 2013, pp. 1–4.
[49] T. Li, M. Rong, X. Wang, and J. Pan, "Experimental investigation on propagation characteristics of PD radiated UHF signal in actual 252 kV GIS," *Energies*, vol. 10, no. 7, p. 942, 2017.
[50] M. Hikita, S. Ohtsuka, J. Wada, S. Okabe, T. Hoshino, and S. Maruyama, "Propagation properties of PD-induced electromagnetic wave in 66 kV GIS model tank with L branch structure," *IEEE Trans. Dielectr. Electr. Insul.*, vol. 18, no. 5, pp. 1678–1685, Oct. 2011.
[51] M. Hikita, S. Ohtsuka, T. Hoshino, S. Maruyama, G. Ueta, and S. Okabe, "Propagation properties of PD-induced electromagnetic wave in GIS model tank with T branch structure," *IEEE Trans. Dielectr. Electr. Insul.*, vol. 18, no. 1, pp. 256–263, Feb. 2011.
[52] R. E. Collin, *Foundation for Microwave Engineering*, 2nd ed. Hoboken, NJ, USA: Wiley, 2001.
[53] T. Li, M. Rong, and X. Wang, "The influence of T-shaped structure on partial discharge radiated electromagnetic wave propagation in GIS," in *Proc. IEEE Region Conf.*, Macao, China, Nov. 2015, pp. 1–4.
[54] M. Rong, T. Li, X. Wang, D. Liu, and A. Zhang, "Investigation on propagation characteristics of PD-induced electromagnetic wave in T-Shaped GIS based on FDTD method," *IEICE Trans. Electron.*, vol. E97-C, no. 9, pp. 880–887, Sep. 2014.
[55] X. Hu, M. D. Judd, and W. H. Siew, "A study of PD location issues in GIS using FDTD simulation," in *Proc. 45th Int. Univ. Power Eng. Conf.*, Aug./Sep. 2010, pp. 1–5.
[56] M. Yoshimura, H. Muto, C. Nishida, M. Kamei, S. Okabe, and S. Kaneko, "Propagation properties of electromagnetic wave through T-branch in GIS," *IEEE Trans. Dielectr. Electr. Insul.*, vol. 14, no. 2, pp. 328–333, Apr. 2007.
[57] S. Kaneko, S. Okabe, M. Yoshimura, H. Muto, C. Nishida, and M. Kamei, "Partial discharge diagnosis method using electromagnetic wave mode transformation in actual GIS structure," *IEEE Trans. Dielectr. Electr. Insul.*, vol. 15, no. 5, pp. 1329–1339, Oct. 2008.
[58] S. Okabe, G. Ueta, H. Hama, T. Ito, M. Hikita, and H. Okubo, "New aspects of UHF PD diagnostics on gas-insulated systems," *IEEE Trans. Dielectr. Electr. Insul.*, vol. 21, no. 5, pp. 2245–2258, Oct. 2014.
[59] S. Okabe, S. Kaneko, M. Yoshimura, H. Muto, C. Nishida, and M. Kamei, "Partial discharge diagnosis method using electromagnetic wave mode transformation in gas insulated switchgear," *IEEE Trans. Dielectr. Electr. Insul.*, vol. 14, no. 3, pp. 702–709, Jun. 2007.
[60] D. Cheng, *Field and Wave Electromagnetics*, 2nd ed. London, U.K.: Pearson, 2006.
[61] T. Li, M. Rong, and X. Wang, "Experimental investigation on UHF partial discharge sensor in GIS," in *Proc. 3rd Int. Conf. Electr. Power Equip.-Switching Technol.*, Oct. 2015, pp. 46–49.
[62] M. Shi, X. Han, X. Zhang, Z. Zhang, and J. Li, "Effect of disconnector and high-voltage conductor on propagation characteristics of PD-induced UHF signals," *IET High Voltage*, vol. 3, no. 3, pp. 187–192, Sep. 2018.
[63] X. Li, X. Wang, D. Xie, X. Wang, A. Yang, and M. Rong, "Time–frequency analysis of PD-induced UHF signal in GIS and feature extraction using invariant moments," *IET Sci., Meas. Technol.*, vol. 12, no. 2, pp. 169–175, Mar. 2018.
[64] M. Hikita, S. Ohtsuka, S. Okabe, J. Wada, T. Hoshino, and S. Maruyama, "Influence of disconnecting part on propagation properties of PD-induced electromagnetic wave in model GIS," *IEEE Trans. Dielectr. Electr. Insul.*, vol. 17, no. 6, pp. 1731–1737, Dec. 2010.
[65] T. Li, M. Rong, D. Liu, X. Wang, and J. Wu, "Experimental research on partial discharge radiated UHF signal attenuation characteristics in GIS," in *Proc. IEEE Int. Conf.*, Oct. 2013, pp. 1–4.
[66] K. Kaiser, *Transmission Lines, Matching, and Crosstalk*. New York, NY, USA: Taylor and Francis, 2006.
[67] M. Hikita, "Fundamental principles and application of diagnosis for GIS using partial discharge measurements," in *Proc. Int. Conf. Elect. Eng. Inform.*, Jul. 2011, pp. 1–6.
[68] M. Talaat, A. El-Zein, and M. Amin, "Developed optimization technique used for the distribution of U-shaped permittivity for cone type spacer in GIS," *Electr. Power Syst. Res.*, vol. 163, pp. 754–766, Oct. 2018.
[69] A. H. Cookson, "Review of high-voltage gas breakdown and insulators in compressed gas," *IEE Proc. A, Phys. Sci., Meas. Instrum., Manage. Educ., Rev.*, vol. 128, no. 4, pp. 303–312, May 1981.
[70] V. Maller and M. Naidu, *Advances in High Voltage Insulation and Arc Interruption in SF6 and Vacuum*. New York, NY, USA: Pergamon, 1981.
[71] S. Okabe, G. Ueta, T. Utsumi, and J. Nukaga, "Insulation characteristics of GIS insulators under lightning impulse with DC voltage superimposed," *IEEE Trans. Dielectr. Electr. Insul.*, vol. 22, no. 6, pp. 1–9, Dec. 2015.
[72] M. Sawada, K. Omori, S. Isejima, S. Ohtsuka, H. Ikeda, M. Hikita, G. Ueta, S. Okabe, T. Hoshino, S. Maruyama, and T. Sakakibara, "Influence of metal flange cover of insulation spacers on propagation properties of PD-induced electromagnetic wave in GIS," in *Proc. Int. Conf. Condition Monit. Diagnosis*, Beijing, China, Apr. 2008, pp. 437–442.
[73] G. Behrmann, K. Wyss, J. Weiss, M. Schraudolph, S. Neuhold, and J. Smajic, "Signal delay effects of solid dielectrics on time-of-flight measurements in GIS," *IEEE Trans. Dielectr. Electr. Insul.*, vol. 23, no. 3, pp. 1275–1284, Jun. 2016.
[74] S. Kaneko, S. Okabe, M. Yoshimura, H. Muto, C. Nishida, and M. Kamei, "Detecting characteristics of various type antennas on partial discharge electromagnetic wave radiating through insulating spacer in gas insulated switchgear," *IEEE Trans. Dielectr. Electr. Insul.*, vol. 16, no. 5, pp. 1462–1472, Oct. 2009.

[75] S. Kaneko, S. Okabe, H. Muto, M. Y. C. Nishida, and M. Kamei, "Electromagnetic wave radiated from an insulating spacer in gas insulated switchgear with partial discharge detection," *IEEE Trans. Dielectr. Electr. Insul.*, vol. 16, no. 1, pp. 60–68, Feb. 2009.
[76] N. Behdad and K. Sarabandi, "Dual resonant slot antennas for wireless applications," in *Proc. IEEE Antennas Propag. Soc. Symp.*, Monterey, CA, USA, vol. 2, Jun. 2004, pp. 1931–1934.
[77] Y. Wang, Z. Wang, and J. Li, "UHF Moore fractal antennas for online GIS PD detection," *IEEE Antennas Wireless Propag. Lett.*, vol. 16, pp. 852–855, 2016.
[78] T. Ju, X. Zhongrong, Z. Xiaoxing, and S. Caixin, "GIS partial discharge quantitative measurements using UHF microstrip antenna sensors," in *Proc. Annu. Rep.-Conf. Elect. Insul. Dielectr. Phenomena*, Vancouver, BC, Canada, Oct. 2007, pp. 116–119.
[79] A. N. Darwish, A. Zakaria, N. Qaddoumi, and L. Albasha, "Low-cost microwave security camera system," in *Proc. 16th Medit. Microw. Symp. (MMS)*, Abu Dhabi, United Arab Emirates, Nov. 2016, pp. 1–4.
[80] W. Stutzman and G. Thiele, *Antenna Theory and Design*, 3rd ed. Hoboken, NJ, USA: Wiley, 2013.
[81] R. Alkadi, A. Shaath, F. Gefe, S. Jaber, N. A. Rayes, A. H. El-Hag, and N. Qaddoumi, "Smart antenna-based partial discharge detection and classification system," in *Proc. 16th Medit. Microw. Symp. (MMS)*, Nov. 2016, pp. 1–4.
[82] W. Yawei, W. Gaungming, and L. Jiangang, "Spiral antenna cuts low profile to 9.4 GHz," *Microw. RF*, vol. 51, no. 11, p. 62, Nov. 2012.
[83] J. Li, "Hilbert fractal antenna for UHF detection of partial discharges in transformers," *IEEE Trans. Dielectr. Electr. Insul.*, vol. 20, no. 6, pp. 2017–2025, Dec. 2013.
[84] J. Li, P. Wang, T. Jiang, L. Bao, and Z. He, "UHF stacked Hilbert antenna array for partial discharge detection," *IEEE Trans. Antennas Propag.*, vol. 61, no. 11, pp. 5798–5801, Nov. 2013.
[85] F. Bin, F. Wang, Q. Sun, S. Lin, Y. Xie, and M. Fan, "Internal UHF antenna for partial discharge detection in GIS," *IET Microw., Antennas, Propag.*, vol. 12, no. 14, pp. 2184–2190, Nov. 2018.
[86] T. Li, M. Rong, C. Zheng, and X. Wang, "Development simulation and experiment study on UHF Partial Discharge Sensor in GIS," *IEEE Trans. Dielectr. Electr. Insul.*, vol. 19, no. 4, pp. 1421–1430, Aug. 2012.
[87] M. Hikita, S. Ohtsuka, T. Teshima, S. Okabe, and S. Kaneko, "Electromagnetic (EM) wave characteristics in GIS and measuring the EM wave leakage at the spacer aperture for partial discharge diagnosis," *IEEE Trans. Dielectr. Electr. Insul.*, vol. 14, no. 2, pp. 453–460, Apr. 2007.
[88] T. Hoshino, S. Maruyama, S. Ohtsuka, M. Hikita, J. Wada, and S. Okabe, "Sensitivity comparison of disc- and loop-type sensors using the UHF method to detect partial discharges in GIS," *IEEE Trans. Dielectr. Electr. Insul.*, vol. 19, no. 3, pp. 910–916, Jun. 2012.
[89] J.-N. Zhang, M.-X. Zhu, Q. Liu, X.-J. Shao, W.-L. He, H. Yao, J.-B. Deng, and G. -J. Zhang, "Design and development of internal UHF sensor for partial discharge detection in GIS," in *Proc. Int. Conf. Condition Monit. Diagnosis (CMD)*, Sep. 2016, pp. 709–712.
[90] A. M. Ishak, M. T. Ishak, M. T. Jusoh, S. F. S. Dardin, and M. D. Judd, "Design and optimization of UHF partial discharge sensors using FDTD modeling," *IEEE Sensors J.*, vol. 17, no. 1, pp. 127–133, Jan. 2017.
[91] T. Hoshino, S. Maruyama, and T. Sakakibara, "Simulation of propagating electromagnetic wave due to partial discharge in GIS using FDTD," in *Proc. Int. Conf. Condition Monit. Diagnosis*, Apr. 2008, pp. 1258–1261.
[92] T. Hoshino, S. Maruyama, and T. Sakakibara, "Simulation of propagating electromagnetic wave due to partial discharge in GIS using FDTD," *IEEE Trans. Power Del.*, vol. 24, no. 1, pp. 153–159, Jan. 2009.

AHMAD DARWISH received the B.S. degree in electrical engineering from the American University of Sharjah (AUS), Sharjah, United Arab Emirates, in 2016, and the M.Eng. degree in electrical engineering from Texas A&M University, College Station, TX, USA, in 2018, where he is currently pursuing the Ph.D. degree. His research interests include high frequency diagnostics, condition monitoring of GIS, ultra high frequency sensors and measurements, electromagnetic interferences, and partial discharge.

SHADY S. REFAAT is currently an Assistant Research Scientist with the Department of Electrical and Computer Engineering, Texas A&M University at Qatar. He was with industry for over twelve years as Electrical Design Engineer. He has published over 50 journal and conference papers. His research interests include electrical machines, power systems, smart grid, energy management systems, reliability of power grid and electric machinery, fault detection, and condition monitoring in conjunction with fault management, and development of fault tolerant systems. He has successfully realized many potential research projects. He is a member of The Institution of Engineering and Technology (IET) and the Smart Grid Center - Extension in Qatar (SGC-Q).

HAMID A. TOLIYAT received the B.S. degree from the Sharif University of Technology, Tehran, Iran, in 1982, the M.S. degree from West Virginia University, Morgantown, WV, USA, in 1986, and the Ph.D. degree from the University of Wisconsin-Madison, Madison, WI, USA, in 1991, all in electrical engineering. He joined the faculty of the Ferdowsi University of Mashhad, Mashhad, Iran, as an Assistant Professor of electrical engineering. In 1994, he joined the Department of Electrical and Computer Engineering, Texas A&M University, where he is currently a Raytheon endowed Professor of electrical engineering. He has supervised more than 85 graduate students, published over 500 technical papers, and presented more than 95 invited lectures all over the world, and has 22 issued and pending US patents. He is the author of three books related to electric machines, control of electrical machines using DSPs, and fault diagnosis of electrical machines. He is a Professional Engineer with the State of Texas. His main research interests and experience include analysis and design of electrical machines, variable speed drives for traction and propulsion applications, fault diagnosis of electric machinery, and magnetic gear integrated electric machines. Dr. Toliyat has received the prestigious Nikola Tesla Field Award for outstanding contributions to the design, analysis, and control of fault-tolerant multiphase electric machines from the IEEE, in 2014, the Cyrill Veinott Award in electromechanical energy conversion from the IEEE Power Engineering Society, in 2004, and many awards from Texas A&M University. He has also received the Space Act Award from NASA, in 1999, and the Schlumberger Foundation Technical Awards, in 2001 and 2000.

HAITHAM ABU-RUB is currently a Full Professor holding two Ph.D.'s. He was with many universities in many countries, including Poland, Palestine, USA, Germany, and Qatar. Since 2006, he has been with Texas A&M University at Qatar. He is the Chair of Electrical and Computer Engineering Program with the Texas A&M University and the Managing Director of Smart Grid Center - Extension in Qatar. His main research interests include electric drives, power electronic converters, renewable energy, and smart grid. He has published more than 350 journal and conference papers, five books and five book chapters. He has supervised many research projects on electric drives, partial discharge, power converters, smart grid topics, and renewable energy systems. Dr. Abu-Rub was a recipient of many national and international awards and recognitions. He was a recipient of the American Fulbright Scholarship and the German Alexander von Humboldt Fellowship.